Neal T. Vogel, MS[1], Jeffrey Annis, PhD[2], Sasha Z. Prisco, MD, PhD[1], Natalia Laixto Mancripe, PhD[3], Madelyn L. Blake[1], Evan L. Brittain, MD, MSCI[2], Kurt W. Prins, MD, PhD[1*], and Felipe Kazmirczak, MD[1*]

* indicates equal contribution

1. Lillehei Heart Institute, Cardiovascular Division, Department of Medicine, University of Minnesota, Minneapolis, MN
2. Division of Cardiovascular Medicine, Department of Medicine, Vanderbilt University Medical Center, Nashville, TN
3. Minnesota Supercomputing Institute, University of Minnesota, Minneapolis, MN

Funding: ELB is funded by NIH R01s FD007627, HL146588, HL163960, HL155278, DK124845, and NIH R61 HL158941. KWP is funded by NIH R01s HL158795 and HL162927.

Authors for Correspondence

Kurt W. Prins, MD, PhD

Associate Professor of Medicine

Director of Translational Research in Pulmonary Hypertension

Lillehei Heart Institute

Department of Medicine, University of Minnesota

And

Felipe Kazmirczak, MD

Assistant Professor of Medicine

Lillehei Heart Institute

Department of Medicine, University of Minnesota

Abstract

Background: Mitochondrial dysfunction, characterized by impaired lipid metabolism and heightened reactive oxygen species (ROS) generation, results in lipid peroxidation-induced ferroptosis. Ferroptosis is an inflammatory mode of cell death as it both promotes complement activation and recruits macrophages. In pulmonary arterial hypertension (PAH), pulmonary arterial endothelial cells exhibit disrupted lipid metabolism and increased ROS production, and there is ectopic complement deposition and inflammatory macrophage accrual in the surrounding vasculature. However, the integrative effects of ferroptosis on metabolism, cellular landscape changes in the lung, complement induction, and pulmonary vascular remodeling are unknown.

Methods: Multi-omics analyses in rodents and a genetic association study in humans evaluated the role of ferroptosis in PAH.

Results: Ferrostatin-1, a small-molecule ferroptosis inhibitor, mitigated PAH severity and improved right ventricular function in monocrotaline rats. RNA-seq and proteomics analyses demonstrated ferroptosis was induced with increasingly severe PAH. Metabolomics and proteomics data showed ferroptosis inhibition restructured lung metabolism and altered phosphatidylcholine and phosphatidylethanolamine levels. RNA-seq, proteomics, and confocal microscopy revealed complement activation and pro-inflammatory cytokines/chemokines were suppressed by ferrostatin-1. Additionally, ferrostatin-1 combatted changes in endothelial, smooth muscle, and interstitial macrophage abundances and gene activation patterns in the lungs as revealed by deconvolution RNA-seq. Finally, the presence of six single-nucleotide polymorphisms in ferroptosis genes were independently associated with pulmonary hypertension severity in the Vanderbilt BioVU repository.

Conclusions: Rodent and human data nominate ferroptosis as a PAH regulating pathway via its ability to modulate lung lipid metabolism, repress pathogenic complement activation, dampen interstitial macrophage infiltration, and restore the lung cellular environment.

Introduction

The accumulation of iron-dependent lipid peroxides induces ferroptosis, a nonapoptotic form of cell death that integrates metabolic derangements, oxidative stress, and inflammation[1]. Multiple organelles regulate ferroptosis, but the mitochondria may be the most important because mitochondria both initiate and propagate ferroptosis[1]. Altered ferroptosis homeostasis occurs in multiple disease states including cancer, sepsis, cardiovascular diseases, and aging, showing the broad implications this mode of cell death has in medicine[1]. The discovery of ferrostatin-1[2] and liproxstatin-1[3], two small molecule inhibitors of ferroptosis, greatly expanded our knowledge of ferroptosis as these molecules exert therapeutic effects in a wide-array of conditions[1]. In the systemic vasculature, ferroptosis induces endothelial cell dysfunction and accelerates atherosclerosis development in mice, and importantly this is suppressed by ferrostatin-1 treatment[4]. In pulmonary arterial hypertension (PAH), pulmonary arterial endothelial cell dysfunction, characterized by disrupted mitochondrial function and impaired iron and lipid metabolism[5], sets up a potentially pro-ferroptotic environment. Small molecule and genetic interventions that suppress ferroptosis reduce PAH severity in rodents[6-8], however a deeper mechanistic understanding of the role of ferroptosis in lung mitochondrial regulation and metabolism is needed to determine how ferroptosis may impact PAH pathogenesis.

In addition to being driven by disrupted metabolism, ferroptosis is a pro-inflammatory mode of cell death[9] that has the potential to drive adverse pulmonary vascular remodeling via modulation of the innate immune system. Ferroptotic cells release damage associated molecular patterns (DAMPs)[9], which can promote ectopic complement deposition[10], a finding present in rodent and human PAH[11]. DAMPs also recruit monocyte derived-macrophage to areas of tissue damage[12], which can further amplify the deleterious pro-inflammatory state. In rodent and human PAH, there is expansion of inflammatory interstitial macrophages, and blocking interstitial macrophage invasion into the lungs dampens PAH severity[13]. At present, the effects of ferroptosis on complement activation and macrophage recruitment in the lungs are unexplored.

To address these important unknowns, we employed a drug intervention approach in translational rodent studies and used quantitative lung proteomics, bulk and deconvolution RNA-sequencing, lung metabolomics, and a human genetic association study to evaluate how ferroptosis modulates lung metabolism, inflammation, and PAH severity.

Results

Ferroptosis Inhibition Mitigated Pulmonary Vascular Remodeling and Improved Right Ventricular Function in Monocrotaline Rats

We first evaluated the physiological effects of ferroptosis in monocrotaline (MCT) rats using a translational approach by starting treatment two weeks after MCT injection. Ferrostatin-1 imparted important therapeutic effects as it increased pulmonary artery acceleration time, reduced right ventricular systolic pressure (RVSP) and end-arterial elastance (Ea), and suppressed small pulmonary arterial remodeling (**Figure 1 A-D**). Accordingly, right ventricular (RV) function as defined by Ees/Ea, tricuspid annular plane systolic excursion (TAPSE), and RV free wall thickening were all improved with ferrostatin-1 (**Figure 1 E-F**). The summation of these data show ferroptosis inhibition combatted pulmonary vascular remodeling and augmented RV function.

RNA-Sequencing and Lung Mitochondrial Proteomics Analyses Identified Links Between Ferroptosis and Pulmonary Hypertension Severity

Next, we used RNA-sequencing and quantitative proteomics analyses of lung samples to perform an unbiased assessment of pathways that were dysregulated as PAH severity increased. Ferroptosis was the second most enriched pathway when delineating pathways associated with higher with Ea (**Figure 2A**). Correlational heatmapping identified multiple positive and significant associations between ferroptotic transcripts and Ea (**Figure 2B and C**). When evaluating pathways induced by higher RVSP, the ferroptosis pathway was not identified in our unbiased assessment (**Supplemental Figure 1**). However, correlational heatmapping demonstrated several ferroptotic transcripts were positively associated with RVSP (**Supplemental Figure 1**).

In our proteomics analysis, multiple metabolic pathways were dysregulated as PAH severity increased . Moreover, the ferroptosis pathway was enriched with increasing Ea and RVSP (**Figure 2 D and G**). Correlational heatmapping identified relationships between multiple ferroptotic proteins and Ea /RVSP (**Figure 2 E and H**). In particular, there were positive correlations between the pro-ferroptotic proteins, voltage-dependent anion-selective channel proteins 2 and 3 (VDAC 2/3), heme oxygenase 1 (HMOX1), and acyl-CoA synthetase long chain family members 1 and 5 (ACSL1/5) and Ea/RVSP (**Figure 2 F and I**). Conversely, the

anti-ferroptotic protein poly(rC)-binding protein 2 was negatively associated with Ea and RVSP (**Figure 2 F and I)**.

Ferrostatin-1 Restructured the Lung Lipidomic Signature

Because our proteomics analysis identified multiple metabolic pathways were associated with pulmonary hypertension severity, we performed a combined metabolomics/lipidomics analysis of whole lung extracts. Both hierarchical cluster analysis and sparse least squares discriminate analysis identified differences in the overall metabolomics/lipidomic signature when the three experimental groups were compared (**Figure 3 A and B**). Random forest classification identified 15 metabolites that differentiated the three groups, and these variables were predominantly lipid species and one amino acid: (glycine) (**Figure 3C**). We subsequently used hierarchical cluster analysis to evaluate ferrostatin-1's effects on three major lipid classes: phophatidylcholines/lysophosphatidylcholines (PC/LPC), phosphatidylethanolamine/ lysophosphatidylethanolamine (PE/LPE), and phosphatidylserine/lysophosphatidylserine (PS/LPS) as these lipids had the most significant differences when the three groups were compared. The most dramatic effects of ferrostatin-1 were on PC/LPC and PE/LPE. Ferrostatin-1 increased multiple PC/LPC species but reduced nearly all PE/LPE (**Figure 3 D and E**). The effects of ferrostatin-1 on PS/LPS were less robust (**Figure 3F**). When profiling amino acids, we found all amino acids other than glycine were elevated in MCT-Veh lungs, which was mostly mirrored in the ferrostatin-1 treatment animals with the exception of valine (**Figure 3G**). Thus, ferroptosis inhibition appeared to have the greatest effect on lung lipid metabolism.

Ferroptosis Inhibition Suppressed Classical Complement Activation and Cytokine Signaling

Next, we probed our ferroptosis-inflammatory hypothesis, which we proposed is mediated by complement activation, by interrogating the coagulation/complement pathway using RNA-seq, proteomics, and immunofluorescence approaches. Hierarchical cluster analysis of RNA-seq data revealed ferrostatin-1 treatment blunted the upregulation of several coagulation/complement transcripts (**Figure 4A**). Correlational heatmapping displayed strong associations between multiple complement transcripts and RVSP and Ea (**Figure 4 B-E**). The transcript abundance of C1QA and C1QB were both correlated with Ea and RVSP (**Figure 4 C and E**). When this pathway was evaluated in our proteomic data, we found ferroptosis inhibition prevented

the upregulation of multiple complement proteins (**Figure 4F**). Correlational heatmapping showed multiple classical complement pathway proteins were associated with RVSP and Ea (**Figure 4 G-J**). To better understand how ferrostatin-1 modulated complement activation in the lungs, we used confocal microscopy to visualize perivascular complement deposition. In agreement with our proteomics and transcriptomics data, perivascular C3 levels in MCT-Veh lungs were significantly elevated as compared to controls, but this response was mitigated by ferrostatin-1 (**Figure 4 K and L**).

Because complement promotes cytokine and chemokine release, we evaluated how ferrostatin-1 impacted the lung inflammatory/cytokine signaling pathway in our RNAseq data. Hierarchical cluster analysis showed ferrostatin-1 reduced the abundance of multiple transcripts in the inflammatory/cytokine pathway as compared to MCT-Veh (**Figure 4M**). In particular, ferrostatin-1 reduced transcript abundance of nodal growth differentiation factor (NODAL), a secreted ligand of the transforming growth factor-beta superfamily of proteins, the transcript that exhibited the strongest relationship with Ea (**Figure 4 N and O**). In addition, ferrostatin-1 lowered transcript levels of tumor necrosis factor receptor superfamily member 11a (TNFRSF11A), a member of the tumor necrosis factor family whose transcript levels were associated with PAH severity (**Figure 4 N and O**). Finally, levels of the pro-inflammatory chemokines including C-X-C motif chemokine ligands (CXCL) 6/10 and C-C motif chemokine ligands (CCL) 9/21 were reduced with ferrostatin-1 (**Figure 4N**). Importantly, CXCL10 and CCL21 levels were positively associated with Ea (**Figure 4O**).

Deconvolution RNA-seq Analysis Revealed Ferrostatin-1 modulated endothelial cell, smooth muscle cell, interstitial macrophage abundance and metabolic and inflammatory phenotypes

To define how ferrostatin-1 modulated the cellular landscape of the pulmonary vasculature, we performed deconvolution RNA-seq analysis to define the changes in cell populations and pathways that were impacted by ferroptosis inhibition. All three experimental groups exhibited distinct cellular compositions in the lungs, and the composition in the ferrostatin-1 treated animals was an intermediate between control and MCT-Veh (**Figure 5A, Supplemental Table 1**). Correlational heatmapping identified relationships between cell types and Ea and RVSP (**Figure 5 B and C**). Cells known to underlie PAH pathobiology including smooth muscle cells, endothelial cells, and interstitial macrophages were strongly associated with Ea and RVSP.

Smooth muscle cells had the most robust correlational relationship with RVSP and Ea. Importantly, ferrostatin-1 treatment mitigated the increase in lung smooth muscle cells when compared to MCT-Veh rats (**Figure 5 D**). Additionally, there were differences in endothelial cell populations when comparing control and MCT-Veh rats (**Figure 5 E and F**). Overall, ferroptosis inhibition partially prevented the reduction of endothelial cells in the EA1 population and the increase in EA2 population. However, the reduction in EA1 as opposed to the increase in EA2 cells was more significantly associated with PAH severity (**Figure 5 E and F**). Additionally, greater abundances of interstitial macrophages were associated with more severe PAH as MCT-Veh rats had the highest numbers of interstitial macrophage (**Figure 5G**). Importantly, ferroptosis inhibition lowered interstitial macrophage numbers as compared to MCT-Veh (**Figure 5G**). Finally, pathway analysis delineated how ferrostatin-1 modulated the transcriptional environment in highly abundant cells. Ferroptosis inhibition suppressed the activation of multiple pathways in both endothelial cells and macrophages. In both cell types, changes in the DNA damage, cellular replication (PI3K,/AKT/MTOR signaling and mitotic spindle), heme metabolism, and lipid handling (adipogenesis) pathways were observed (**Figure 5H**).

Presence of single-nucleotide polymorphisms in ferroptosis genes was associated with more severe pulmonary hypertension

Finally, we evaluated how the presence of single-nucleotide polymorphisms (SNPs) in ferroptosis genes impacted noninvasive and invasive measures of pulmonary hypertension in a mixed cohort of patients evaluated at the Vanderbilt BioVU biorepository. The presence of six SNPs in ferroptosis genes (**Supplemental Table 2**) were associated with more severe pulmonary hypertension, however the overall frequency was low. Therefore, we pooled all six SNPs and compared how carriers of ferroptosis SNPs compared to those lacking potentially pathogenic SNPs. In an unadjusted analysis, carriers had significantly higher right ventricular systolic pressure [Carriers: 63.9 (45.0-80.6), Noncarriers 46.8 (35.0-62.0)] as determined by echocardiography (**Figure 6A**). Furthermore, invasively measured mean pulmonary arterial pressure [Carriers: 40.0 (25.0-51.0), Noncarriers 31.0 (22.0-41.0)], and pulmonary vascular resistance [Carriers: 4.3 (2.4-6.9), Noncarriers 2.6 (1.7-4.6)] were higher in those harboring ferroptosis SNPs (**Figure 6 B-C**). Because this was a mixed cohort, we performed a multivariate regression analysis and even after

correcting for age, sex, presence of heart failure and chronic obstructive pulmonary disease; ferroptotic SNPs were independently associated with higher RVSP, mPAP, and PVR (**Figure 6 D-E**). Thus, we provide human data demonstrating associations between ferroptosis and pulmonary hypertension severity .

Discussion

In summary, our translational rodent studies show small molecule inhibition of ferroptosis mitigates PAH and improves right ventricular function in MCT rats. Transcriptomics and proteomics analyses demonstrate a relationship between ferroptosis induction and PAH, which provides unbiased data to support our physiological findings. Our metabolomics/lipidomics experiments suggest ferrostatin-1 most robustly modulates lung lipid metabolism with particular changes in phophatidylcholines and phosphatidylethanonlamines species. In the pulmonary vasculature, suppression of ferroptosis alters endothelial and pulmonary artery smooth muscle cell numbers and gene activation patterns. Additionally, ferrostatin-1 mitigates pathological immune activation in the lung by suppressing perivascular complement deposition, lowering cytokines and chemokines, and reducing interstitial macrophage abundance. Finally, human studies reveal the presence of SNPs in ferroptosis genes is associated with more severe pulmonary vascular disease burden, and that association remains even after adjusting for relevant clinical co-morbid conditions. Our proposed model is ferroptotic pulmonary endothelial cell releases DAMPs that activate complement and recruit pro-inflammatory macrophage. These changes in-turn promote pulmonary artery smooth muscle cell proliferation and subsequent pulmonary hypertension (**Figure 7**).

Our findings that ferroptosis induces both metabolic derangements and pathological inflammation in the lungs has potential to link two heavily implicated molecular phenotypes in PAH pathology to one targetable pathway. In PAH, derangements in lung metabolism including altered fatty acid oxidation[14,15], heightened anaerobic glucose metabolism[16], and disrupted amino acid utilization[17-19] are well documented. Interesting, ferroptosis has the potential to impact several catabolic pathways via its ability to suppress electron transport chain activity[20], a final common pathway for nearly all metabolic processes. While targeting specific metabolic arms including suppression of fatty acid oxidation[14] and activation of glucose oxidative metabolism[21] have robust therapeutic effects in preclinical PAH, the translation of these studies to humans has not been met with overwhelming success[22]. Perhaps, targeting just one isolated branch of metabolism is insufficient to counteract human PAH pathogenesis, and more broad-based metabolic interventions, such as ferroptosis inhibition, would garner greater success. The observation that ferroptosis antagonism also combats ectopic complement activation, lowers levels of several cytokines/chemokines, and mitigates macrophage infiltration suggests its anti-inflammatory properties conferred beneficial effects in the pulmonary vasculature. While there is strong

data showing many individual cell types or cytokines/chemokines promote PAH in rodents[23]; unfortunately the translation of these findings to humans has not been as fruitful as desired. In particular, antagonism of interleukin-6 signaling with tocilizumab[24] or depletion of B-cells with rituximab[25] did not significantly change PAH severity in small clinical trials. Perhaps suppressing an individual cytokine or immune cell type may not be the most effective therapy in humans as the available data suggests there is widespread immune activation in PAH[23]. Moreover, the cross-talk between immune cells and pulmonary vascular cells is crucial in PAH progression as there is greater immune-pulmonary vascular interactions in hereditary PAH as compared to idiopathic PAH, and this finding correlates with hemodynamic severity[26]. Because our data suggests ferroptosis both dampens mitochondrial metabolism and initiates innate immune system activation in the pulmonary vasculature, approaches to counteract ferroptosis may lead to greater translational success in future studies.

While our study shows ferrostatin-1 mitigates PAH severity in MCT rats, there are additional preclinical and human data that support our hypothesis that ferroptosis promotes pulmonary hypertension. First, several ferropto sis-suppressing molecules exhibit therapeutic efficacy in relevant preclinical models of pulmonary vascular disease including MCT rats, Sugen-hypoxia rats, chronic hypoxia rats, and lambs with persistent pulmonary hypertension of the newborn (**Table 1**). In addition, KEGG pathway analysis of upregulated transcripts in PAH endothelial cells analyzed by single cell RNA-seq[27] identifies ferroptosis as the pathway with the greatest enrichment (**Supplemental Figure 2**). Furthermore, a proteomic study shows there is a 35% reduction in glutathione peroxidase-4, an anti-ferroptotic protein, in pulmonary arterial endothelial cells from PAH patients[28]. Finally, there are higher systemic levels of lipid peroxidation in PAH patients as urinary abundance of isoprostaglandin F2a are significantly higher than controls[29]. The summation of our data, other published work, and human studies suggests ferroptosis may be a targetable pathway to suppress adverse pulmonary vascular remodeling.

In our proteomics analysis of the lungs, we highlighted differences in multiple metabolic pathways with ferroptosis inhibition. However, the metabolomics/lipidomics analysis suggested the greatest effect of ferrostatin-1 was on lipid metabolism. In particular, ferrostatin-1 increases levels of multiple phosphatidylcholines (**Figure 3**), which may have direct relevance to mitochondrial function because phosphatidylcholines are a major component of the mitochondrial membrane system[30]. Perhaps the greater

concentrations of phosphatidylcholines contributes to the proteomic changes in other metabolic pathways via the stabilization and preservation of mitochondria. In addition, phosphatidylcholines are required for inner membrane protein translocases in the mitochondria[30]. A change in phosphatidylcholines could also alter mitochondrial protein stability as matrix and inner membrane proteins may not be properly trafficked into the mitochondria in the PAH lung due to the dysregulation of phosphatidylcholines. Additionally, ferrostatin-1 lowered the levels of nearly all phosphatidylethanolamines profiled (**Figure 3**). This may be an important feedback mechanism to mitigate ferroptosis because peroxidation of phosphatidylethanolamine is crucial for ferroptosis initiation[31]. Surprisingly, ferrostatin-1 had almost no effect on lung amino acid abundances with the exception of reducing levels of valine, a branched chain amino acid. While amino acids regulate ferroptosis homeostasis in other conditions[32], our data suggests amino acids do not play a dominant role in ferroptosis induction in PAH. In conclusion, the strongest effects of ferrostatin-1 on lung metabolism appears to be on lipid homeostasis, and these changes may underlie some of the beneficial physiological effects of ferroptosis antagonism.

Our deconvolution RNA-seq analysis identifies changes in endothelial cell, smooth muscle cell, and interstitial macrophage number and gene activation patterns. However, other immune cell types undoubtedly contribute to pulmonary vascular remodeling, but our approach was not sensitive enough to detect changes in these lower abundant immune cell populations. Certainly, there is literature demonstrating T-cells[33] and B-cells[34] play important roles in pulmonary vascular remodeling, however we did not detect changes in these cell populations with ferroptosis inhibition (**Supplemental Table 1**). In addition, we did not see a profound change in mast cell numbers with ferrostatin-1 treatment (**Supplemental Table 1**). With the limitations of our approach, it appears ferroptosis inhibition exerted the greatest effects on endothelial cells, smooth muscle cells, and recruited macrophage.

Our work has important limitations that we must acknowledge. First, we used whole lung tissue in our proteomics and metabolomics analyses, and defining what cell types are contributing to the observed changes can not be determined. We tried to overcome some of these limitations by using deconvolution RNA-seq to define changes in cell numbers and gene activation patterns. Moreover, our SNP analysis was conducted in a mixed population of patients and not only in PAH patients. When we mined the UK Biobank, our proposed pathogenic SNPs were in very low abundance, and they were not associated with differences in PAH severity

(data not shown). There are at least three potential reasons for the lack of congruent findings including 1) sample size, 2) ferroptosis may have a differing role in all distinct PAH etiologies, or 3) it may due to differences in ethnicities and genetic lineages between the two cohorts. In support of hypothesis 3, we found distinct racial differences when comparing ferroptosis SNP carriers (greater proportion of blacks) to those lacking SNPs in the BioVU cohort (**Supplemental Table 3**)

Figure 1: Ferrostatin-1 Treatment Combatted Pulmonary Hypertension Severity and Improved Right Ventricular Function in Monocrotaline Rats. (A) Ferrostatin-1 treatment increased pulmonary artery acceleration time in MCT rats (Con: 26±1, MCT-V: 16±1, MCT-Fer-1: 21±1 ms). (B) Ferroptosis inhibition with ferrostatin-1 reduced right ventricular systolic pressure (RVSP) (Con: 21±1, MCT-V: 69±7, MCT-Fer-1: 46±2 mmHg), *p*-values determined by Kruskal-Wallis test (C) End-arterial elastance (E_a) was lowered by ferroptosis inhibition (Con: 0.08±0.02, MCT-V: 0.40±0.04, MCT-Fer-1: 0.25±0.02 mmHg/μL), *p*-values determined by Kruskal-Wallis test. (D) Small vessel pulmonary arterial remodeling was blunted by ferrostatin-1 [Median, (25th-75th%), Con: 25.8, (21.5-29.3), MCT-V: 43.8, (38.5-49.5), MCT-Fer-1: 23.9%, (20.5-34.7), *p*-values determined by Kruskal-Wallis test]. (E) Ferrostatin-1 treated improved right ventricular-pulmonary artery coupling (E_{es}/E_a) (Con: 1.3±0.2, MCT-V: 0.37±0.04, MCT-Fer-1: 0.88±0.08, *p*-values determined by Brown-Forsythe and Welch ANOVA test), TAPSE (F), and RV free wall thickening (G).

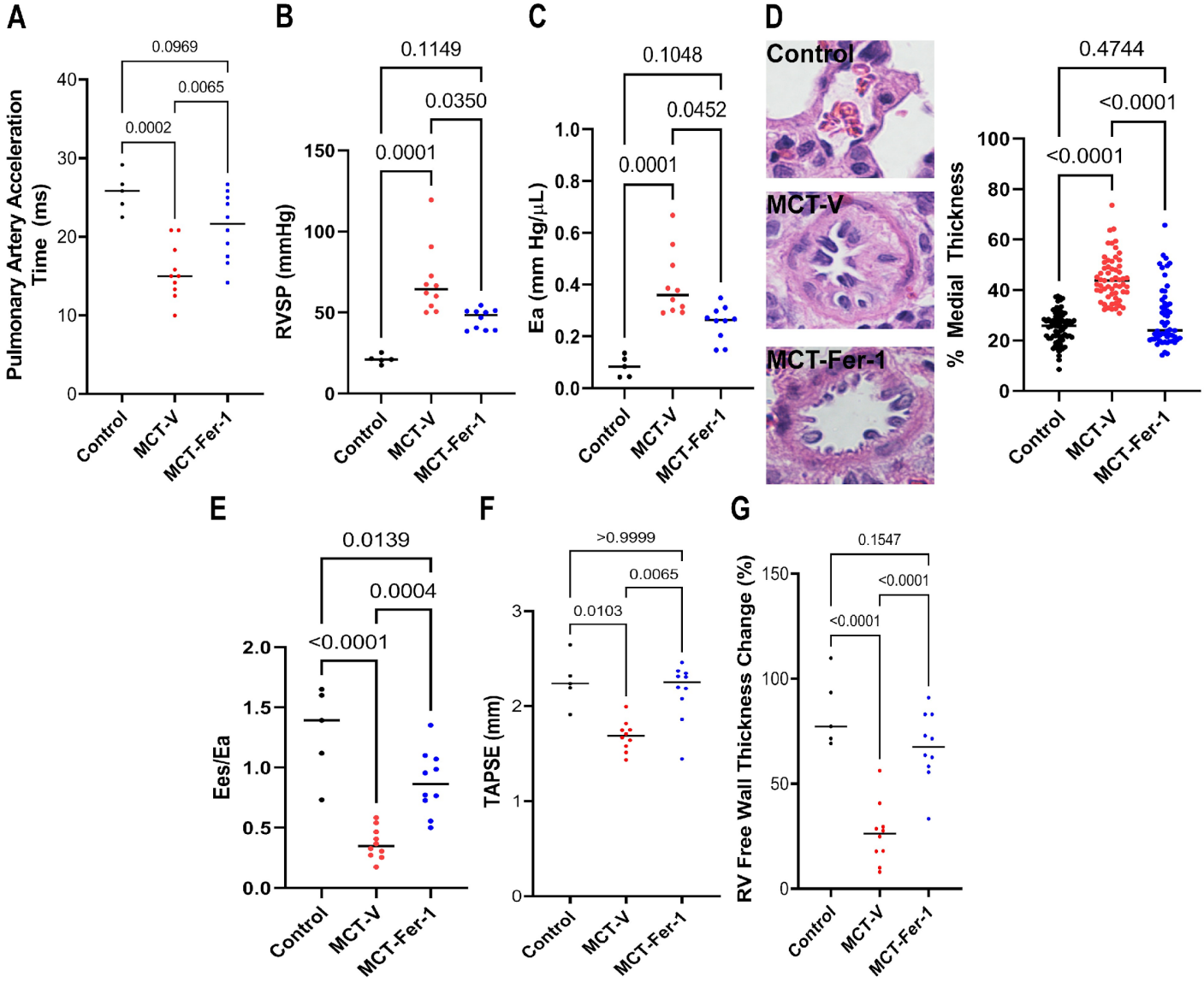
A
Pulmonary Artery Acceleration Time (ms)
0.0969
0.0065
0.0002
Control
MCT-V
MCT-Fer-1
B
RVSP (mmHg)
0.1149
0.0350
0.0001
C
Ea (mm Hg/μL)
0.1048
0.0452
0.0001
D
Control
MCT-V
MCT-Fer-1
% Medial Thickness
0.4744
<0.0001
<0.0001
E
Ees/Ea
0.0139
0.0004
<0.0001
F
TAPSE (mm)
>0.9999
0.0065
0.0103
G
RV Free Wall Thickness Change (%)
0.1547
<0.0001
<0.0001

Figure 2: Lung RNAsequencing and Proteomics Analyses Identified Associations Between Ferroptosis and Pulmonary Hypertension Severity. (A) Pathway analysis of transcripts significantly associated with Ea. (B) Correlational heat mapping of ferroptosis pathway transcripts and Ea. (C) Ten transcripts most strongly associated with Ea. (D) Pathway analysis of proteins significantly associated with Ea. (E) Correlational heat map of ferroptosis proteins with Ea. (F) Ferroptosis proteins most strongly associated with Ea. (G) Pathway analysis of proteins significantly associated with right ventricular systolic pressure (RVSP). (H) Correlational heat map of ferroptosis proteins and RVSP. (I) Ten most strongly associated proteins with RVSP.

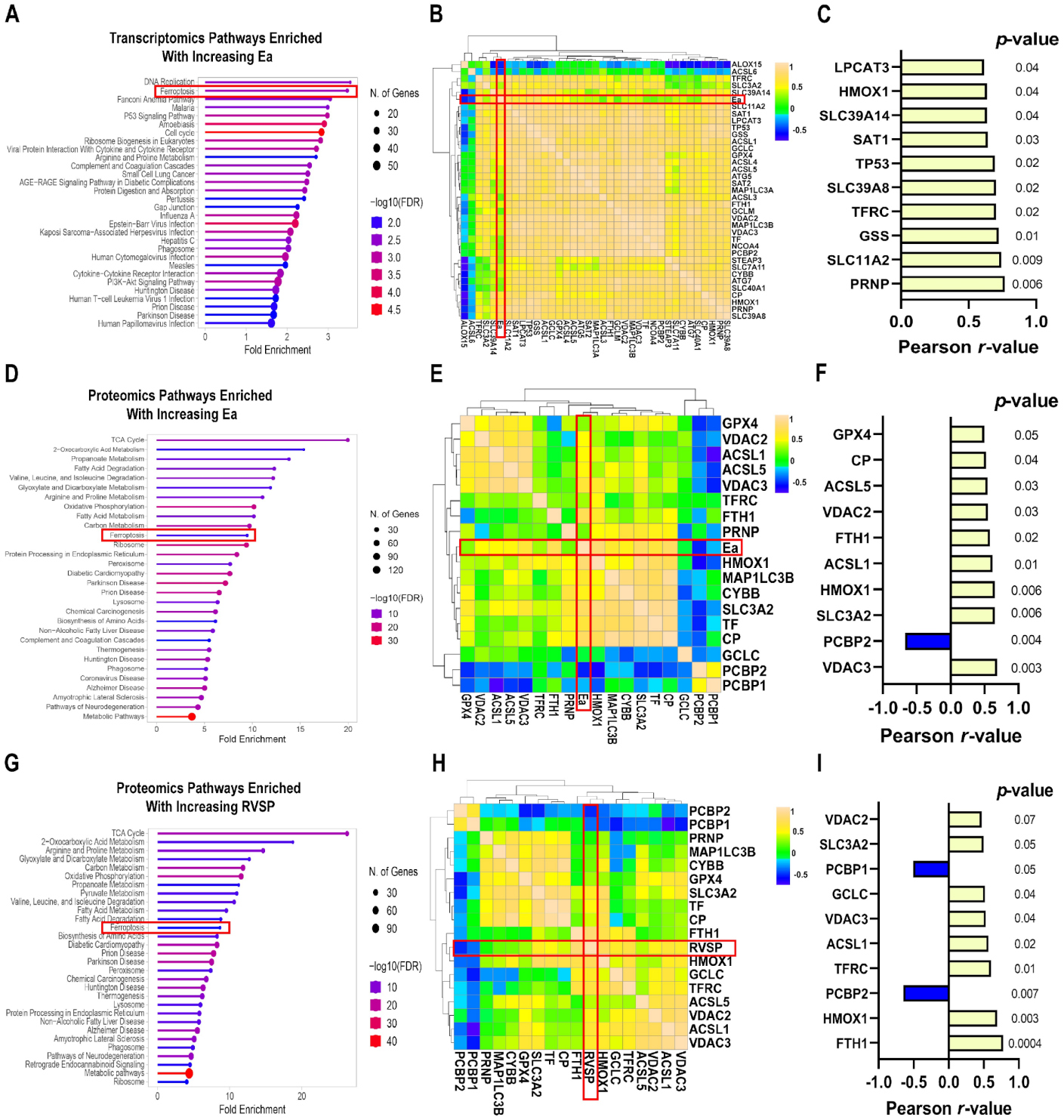
A
Transcriptomics Pathways Enriched With Increasing Ea
DNA Replication
Ferroptosis
Fanconi Anemia Pathway
Malaria
P53 Signaling Pathway
Amoebiasis
Cell cycle
Ribosome Biogenesis in Eukaryotes
Viral Protein Interaction With Cytokine and Cytokine Receptor
Arginine and Proline Metabolism
Complement and Coagulation Cascades
Small Cell Lung Cancer
AGE-RAGE Signaling Pathway in Diabetic Complications
Protein Digestion and Absorption
Pertussis
Gap Junction
Influenza A
Epstein-Barr Virus Infection
Kaposi Sarcoma-Associated Herpesvirus Infection
Hepatitis C
Phagosome
Human Cytomegalovirus Infection
Measles
Cytokine-Cytokine Receptor Interaction
PI3K-Akt Signaling Pathway
Huntington Disease
Human T-cell Leukemia Virus 1 Infection
Prion Disease
Parkinson Disease
Human Papillomavirus Infection
0 1 2 3
Fold Enrichment
N. of Genes
20
30
40
50
-log10(FDR)
2.0
2.5
3.0
3.5
4.0
4.5
B
ALOX15
ACSL6
TFRC
SLC3A2
SLC39A14
Ea
SLC11A2
SAT1
LPCAT3
TP53
GSS
ACSL1
GCLC
GPX4
ACSL4
ACSL5
ATG5
SAT2
MAP1LC3A
ACSL3
FTH1
GCLM
VDAC2
MAP1LC3B
VDAC3
TF
NCOA4
PCBP2
STEAP3
SLC7A11
CYBB
ATG7
SLC40A1
CP
HMOX1
PRNP
SLC39A8
1
0.5
0
-0.5
C
p-value
LPCAT3 0.04
HMOX1 0.04
SLC39A14 0.04
SAT1 0.03
TP53 0.02
SLC39A8 0.02
TFRC 0.02
GSS 0.01
SLC11A2 0.009
PRNP 0.006
0.0 0.5 1.0
Pearson r-value
D
Proteomics Pathways Enriched With Increasing Ea
TCA Cycle
2-Oxocarboxylic Acid Metabolism
Propanoate Metabolism
Fatty Acid Degradation
Valine, Leucine, and Isoleucine Degradation
Glyoxylate and Dicarboxylate Metabolism
Arginine and Proline Metabolism
Oxidative Phosphorylation
Fatty Acid Metabolism
Carbon Metabolism
Ferroptosis
Ribosome
Protein Processing in Endoplasmic Reticulum
Peroxisome
Diabetic Cardiomyopathy
Parkinson Disease
Prion Disease
Lysosome
Chemical Carcinogenesis
Biosynthesis of Amino Acids
Non-Alcoholic Fatty Liver Disease
Complement and Coagulation Cascades
Thermogenesis
Huntington Disease
Phagosome
Coronavirus Disease
Alzheimer Disease
Amyotrophic Lateral Sclerosis
Pathways of Neurodegeneration
Metabolic Pathways
0 5 10 15 20
Fold Enrichment
N. of Genes
30
60
90
120
-log10(FDR)
10
20
30
E
GPX4
VDAC2
ACSL1
ACSL5
VDAC3
TFRC
FTH1
PRNP
Ea
HMOX1
MAP1LC3B
CYBB
SLC3A2
TF
CP
GCLC
PCBP2
PCBP1
1
0.5
0
-0.5
F
p-value
GPX4 0.05
CP 0.04
ACSL5 0.03
VDAC2 0.03
FTH1 0.02
ACSL1 0.01
HMOX1 0.006
SLC3A2 0.006
PCBP2 0.004
VDAC3 0.003
-1.0 -0.5 0.0 0.5 1.0
Pearson r-value
G
Proteomics Pathways Enriched With Increasing RVSP
TCA Cycle
2-Oxocarboxylic Acid Metabolism
Arginine and Proline Metabolism
Glyoxylate and Dicarboxylate Metabolism
Carbon Metabolism
Oxidative Phosphorylation
Propanoate Metabolism
Pyruvate Metabolism
Valine, Leucine, and Isoleucine Degradation
Fatty Acid Metabolism
Fatty Acid Degradation
Ferroptosis
Biosynthesis of Amino Acids
Diabetic Cardiomyopathy
Prion Disease
Parkinson Disease
Peroxisome
Chemical Carcinogenesis
Huntington Disease
Thermogenesis
Lysosome
Protein Processing in Endoplasmic Reticulum
Non-Alcoholic Fatty Liver Disease
Alzheimer Disease
Amyotrophic Lateral Sclerosis
Phagosome
Pathways of Neurodegeneration
Retrograde Endocannabinoid Signaling
Metabolic pathways
Ribosome
0 10 20
Fold Enrichment
N. of Genes
30
60
90
-log10(FDR)
10
20
30
40
H
PCBP2
PCBP1
PRNP
MAP1LC3B
CYBB
GPX4
SLC3A2
TF
CP
FTH1
RVSP
HMOX1
GCLC
TFRC
ACSL5
VDAC2
ACSL1
VDAC3
1
0.5
0
-0.5
I
p-value
VDAC2 0.07
SLC3A2 0.05
PCBP1 0.05
GCLC 0.04
VDAC3 0.04
ACSL1 0.02
TFRC 0.01
PCBP2 0.007
HMOX1 0.003
FTH1 0.0004
-1.0 -0.5 0.0 0.5 1.0
Pearson r-value

Figure 3: Combined Metabolomics/Lipidomics Profiling of Whole Lungs Identified Changes in Lipid Metabolism with Ferrostatin-1. (A) Hierarchical cluster analysis of the most divergently regulated 250 metabolites in the lungs. (B) Sparse least squares discriminant analysis highlighted differences in the three experimental groups. (C) Random forest classification identified the top 15 most important metabolites for differentiating the three groups. Lipid species dominated the changes in the lung. (D) Hierarchical cluster analysis of lysophophatidylcholines (LPC) and phosphitidylcholines (PC). Ferrostatin-1 treatment increased a subpopulation of LPC and PC. (E) Hierarchical cluster analysis showed ferrostatin-1 reduced almost all LPE/PE species. Lung LPS+PS (F) and amino acids (G) levels were minimally altered by ferrostatin-1 treatment as compared to MCT-Vehicle. CE: Cholesterol ester, HxCer: Hexosylceramide, PE: phosphatidylethanolamine, LPC: Lysophophatidylcholine, PC: Phosphatidylcholine, PS: Phosphatidylserine, PA: Phosphatidic acid.

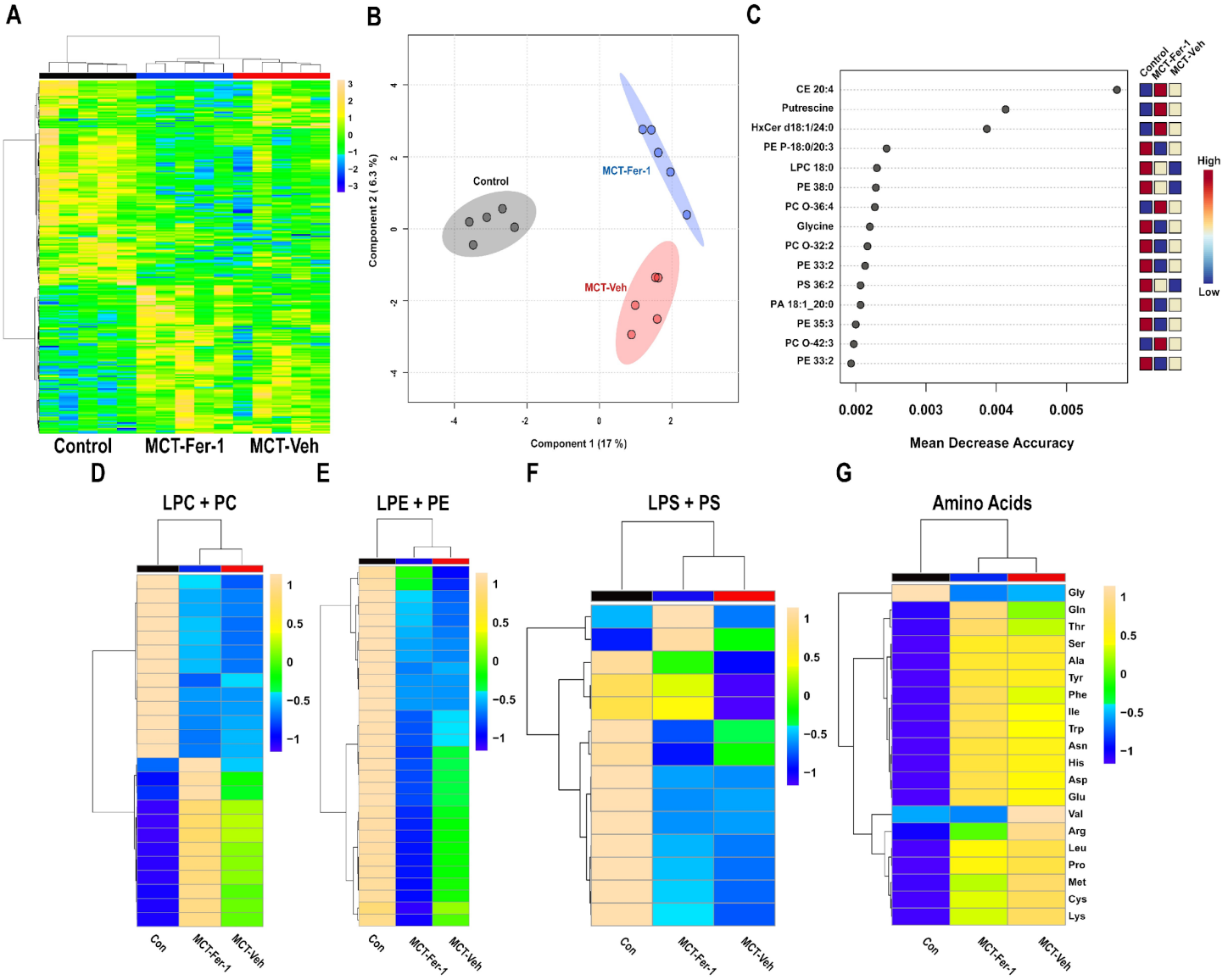
A
Control
MCT-Fer-1
MCT-Veh
B
Control
MCT-Fer-1
MCT-Veh
Component 2 (6.3 %)
Component 1 (17 %)
C
CE 20:4
Putrescine
HxCer d18:1/24:0
PE P-18:0/20:3
LPC 18:0
PE 38:0
PC O-36:4
Glycine
PC O-32:2
PE 33:2
PS 36:2
PA 18:1_20:0
PE 35:3
PC O-42:3
PE 33:2
Control
MCT-Fer-1
MCT-Veh
High
Low
0.002
0.003
0.004
0.005
Mean Decrease Accuracy
D
LPC + PC
E
LPE + PE
F
LPS + PS
G
Amino Acids
Gly
Gln
Thr
Ser
Ala
Tyr
Phe
Ile
Trp
Asn
His
Asp
Glu
Val
Arg
Leu
Pro
Met
Cys
Lys
Con
MCT-Fer-1
MCT-Veh

Figure 4: Ferroptosis Mitigated Complement Activation and Cytokine Signaling in the Lungs of MCT Rats (A) Hierarchical cluster analysis of transcripts in the complement coagulation pathway. Ferrostatin-1 reduced levels of many transcripts as compared to MCT-Veh. (B) Correlational heat map of complement/coagulation transcripts with Ea. (C) Identification of 10 transcripts most strongly associated with Ea. Classical complement components C1Qa and C1Qb were higher as Ea increased. (D) Correlational heat map of complement/coagulation transcripts with RVSP. (E) Ten transcripts most strongly associated with RVSP. (F) Hierarchical cluster analysis of proteins in the complement/coagulation cascade. (G) Correlational heat map of complement/coagulation proteins with Ea. (H) Identification of 10 proteins most strongly associated with Ea. (I) Correlational heat map of complement/coagulation proteins with RVSP. (J) Identification of 10 proteins most strongly associated with RVSP. (K) Representative confocal micrographs showed increased complement deposition around the pulmonary vasculature in MCT-Vehicle, which was mitigated by ferrostatin-1. (L) Quantification of perivascular C3 intentisty. *p*-values determined by Kruskal-Wallis test and Dunn's multiple comparisons test. (M) Hierarchical cluster analysis of the inflammatory/cytokine pathway form lung extracts. (N) Random forest classification shows multiple inflammatory cytokines are reduced by ferrostatin-1 treatment and that helps differentiate the three groups. (O) 15 inflammatory/cytokine transcripts that were most strongly associated with Ea. Red boxes outline classical complement components.

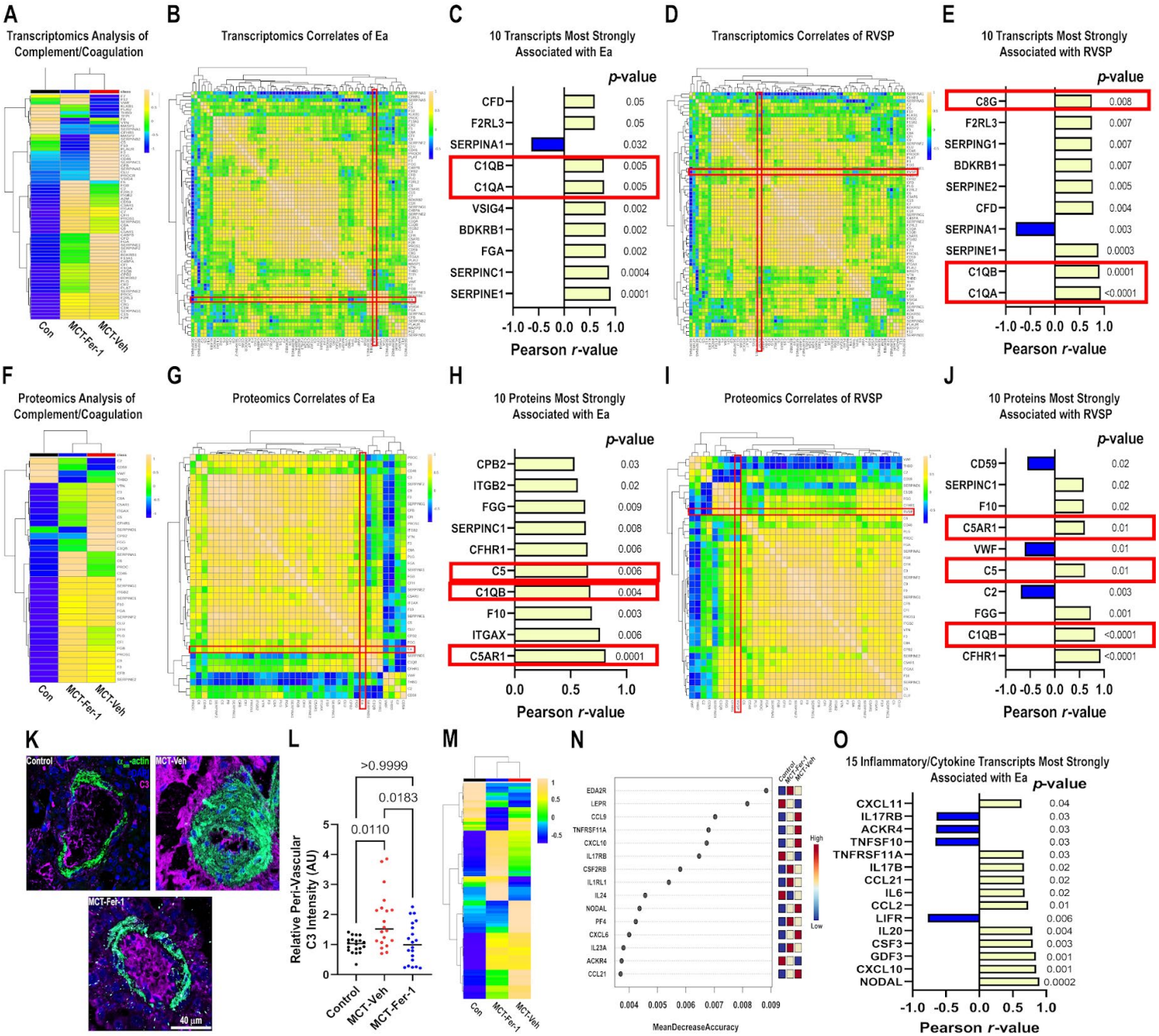
A
Transcriptomics Analysis of Complement/Coagulation
Con
MCT-Fer-1
MCT-Veh
B
Transcriptomics Correlates of Ea
C
10 Transcripts Most Strongly Associated with Ea
p-value
CFD 0.05
F2RL3 0.05
SERPINA1 0.032
C1QB 0.005
C1QA 0.005
VSIG4 0.002
BDKRB1 0.002
FGA 0.002
SERPINC1 0.0004
SERPINE1 0.0001
-1.0 -0.5 0.0 0.5 1.0
Pearson r-value
D
Transcriptomics Correlates of RVSP
E
10 Transcripts Most Strongly Associated with RVSP
p-value
C8G 0.008
F2RL3 0.007
SERPING1 0.007
BDKRB1 0.007
SERPINE2 0.005
CFD 0.004
SERPINA1 0.003
SERPINE1 0.0003
C1QB 0.0001
C1QA <0.0001
-1.0 -0.5 0.0 0.5 1.0
Pearson r-value
F
Proteomics Analysis of Complement/Coagulation
Con
MCT-Fer-1
MCT-Veh
G
Proteomics Correlates of Ea
H
10 Proteins Most Strongly Associated with Ea
p-value
CPB2 0.03
ITGB2 0.02
FGG 0.009
SERPINC1 0.008
CFHR1 0.006
C5 0.006
C1QB 0.004
F10 0.003
ITGAX 0.006
C5AR1 0.0001
0.0 0.5 1.0
Pearson r-value
I
Proteomics Correlates of RVSP
J
10 Proteins Most Strongly Associated with RVSP
p-value
CD59 0.02
SERPINC1 0.02
F10 0.02
C5AR1 0.01
VWF 0.01
C5 0.01
C2 0.003
FGG 0.001
C1QB <0.0001
CFHR1 <0.0001
-1.0 -0.5 0.0 0.5 1.0
Pearson r-value
K
Control
MCT-Veh
MCT-Fer-1
40 µm
L
>0.9999
0.0183
0.0110
Relative Peri-Vascular C3 Intensity (AU)
Control
MCT-Veh
MCT-Fer-1
M
Con
MCT-Fer-1
MCT-Veh
N
EDA2R
LEPR
CCL9
TNFRSF11A
CXCL10
IL17RB
CSF2RB
IL1RL1
IL24
NODAL
PF4
CXCL6
IL23A
ACKR4
CCL21
Control
MCT-Fer-1
MCT-Veh
High
Low
0.004 0.005 0.006 0.007 0.008 0.009
MeanDecreaseAccuracy
O
15 Inflammatory/Cytokine Transcripts Most Strongly Associated with Ea
p-value
CXCL11 0.04
IL17RB 0.03
ACKR4 0.03
TNFSF10 0.03
TNFRSF11A 0.03
IL17B 0.02
CCL21 0.02
IL6 0.02
CCL2 0.01
LIFR 0.006
IL20 0.004
CSF3 0.003
GDF3 0.001
CXCL10 0.001
NODAL 0.0002
-1.0 -0.5 0.0 0.5 1.0
Pearson r-value

Figure 5: Deconvolution RNA-sequencing Demonstrated Ferroptosis Inhibition Modulated Endothelial, Smooth Muscle, and Interstitial Macrophage Abundance and Gene Activation Patterns. (A) Map of cell type abundances in control, MCT-Veh, and MCT-Fer-1 animals as determined by deconvolution RNAseq. Correlational heat mapping identified relationships between cell type abundances and Ea (B) and RVSP (C). Relationships between smooth muscle cell abundance and Ea and RVSP. (D) Relationships between endothelial cell population 1 (EA1) and Ea and RVSP. (F) Relationships between endothelial cell population 2 (EA2) and Ea and RVSP. (G) Relationships between interstitial macrophage population and Ea and RVSP. (H) Pathway analysis of transcriptomic changes in endothelial cells, macrophage, and total cells with ferrostatin-1 treatment.

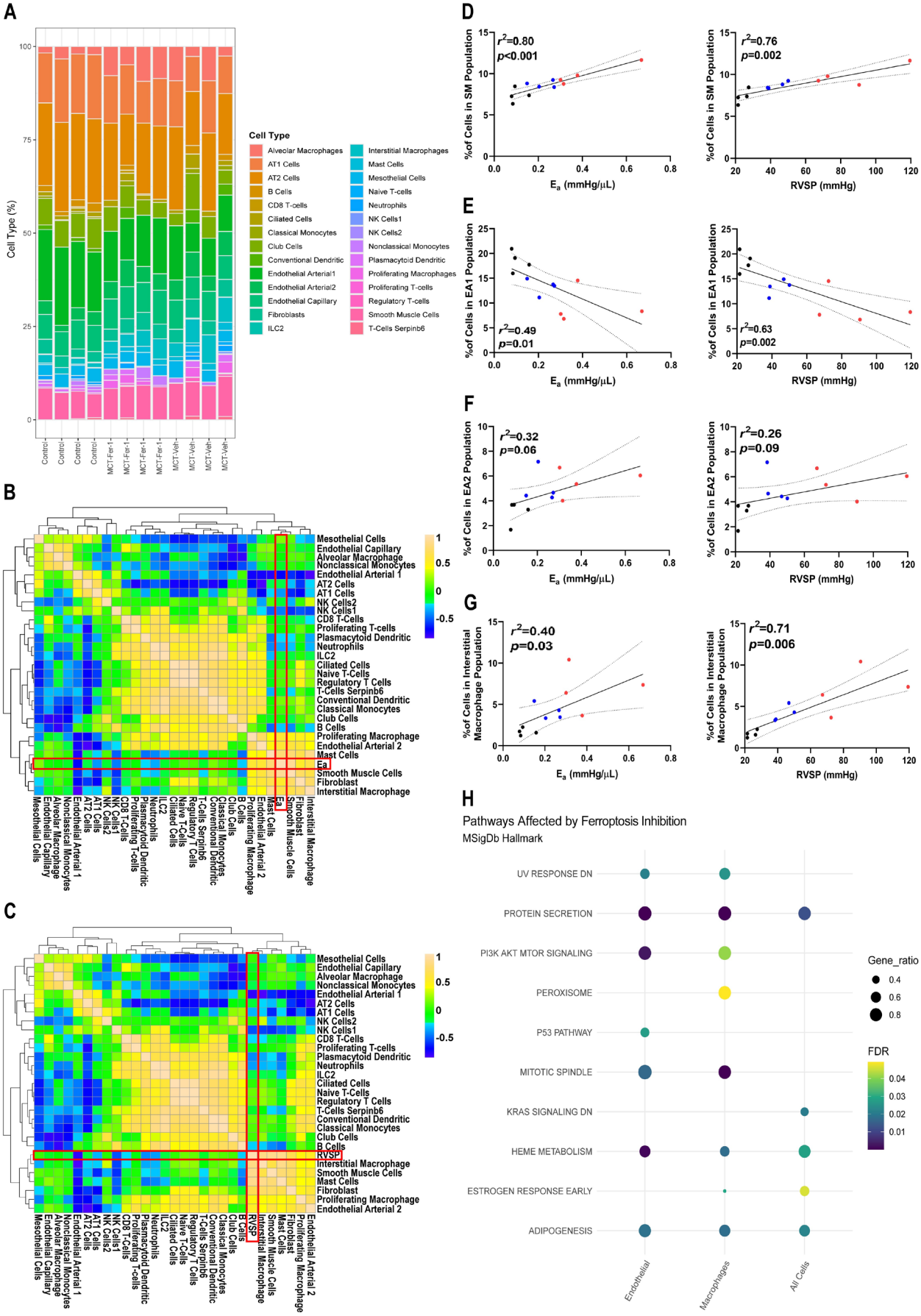
A
Cell Type (%)
Control
MCT-Fer-1
MCT-Veh
Cell Type
Alveolar Macrophages
AT1 Cells
AT2 Cells
B Cells
CD8 T-cells
Ciliated Cells
Classical Monocytes
Club Cells
Conventional Dendritic
Endothelial Arterial1
Endothelial Arterial2
Endothelial Capillary
Fibroblasts
ILC2
Interstitial Macrophages
Mast Cells
Mesothelial Cells
Naive T-cells
Neutrophils
NK Cells1
NK Cells2
Nonclassical Monocytes
Plasmacytoid Dendritic
Proliferating Macrophages
Proliferating T-cells
Regulatory T-cells
Smooth Muscle Cells
T-Cells Serpinb6
B
C
D
r^2=0.80
p<0.001
r^2=0.76
p=0.002
%of Cells in SM Population
E_a (mmHg/μL)
RVSP (mmHg)
E
r^2=0.49
p=0.01
r^2=0.63
p=0.002
%of Cells in EA1 Population
F
r^2=0.32
p=0.06
r^2=0.26
p=0.09
%of Cells in EA2 Population
G
r^2=0.40
p=0.03
r^2=0.71
p=0.006
%of Cells in Interstitial Macrophage Population
H
Pathways Affected by Ferroptosis Inhibition
MSigDb Hallmark
UV RESPONSE DN
PROTEIN SECRETION
PI3K AKT MTOR SIGNALING
PEROXISOME
P53 PATHWAY
MITOTIC SPINDLE
KRAS SIGNALING DN
HEME METABOLISM
ESTROGEN RESPONSE EARLY
ADIPOGENESIS
Endothelial
Macrophages
All Cells
Gene_ratio
FDR

Figure 6: Presence of SNPs in Ferroptosis Regulating Genes Was Associated With More Severe Pulmonary Hypertension. (A) Patients harboring SNPs in ferroptosis genes had higher right ventricular systolic pressures [Carriers: 63.9 (45.0-80.6), Noncarriers 46.8 (35.0-62.0), median (25th-75th percentiles)] as determined by echocardiography, (B) invasively measured mean pulmonary arterial pressure [Carriers: 40.0 (25.0-51.0), Noncarriers 31.0 (22.0-41.0), median (25th-75th percentiles)], and pulmonary vascular resistance [Carriers: 4.3 (2.4-6.9), Noncarriers 2.6 (1.7-4.6), median (25th-75th percentiles)] as determined by invasive hemodynamic studies (C). *p*-values as determined by Mann-Whitney U-test. Forest plots depicted correlational co-efficient with standard errors and calculated *p*-values when RVSP (D), mPAP (E), and PVR (F) were modeled in multivariate regression analysis.

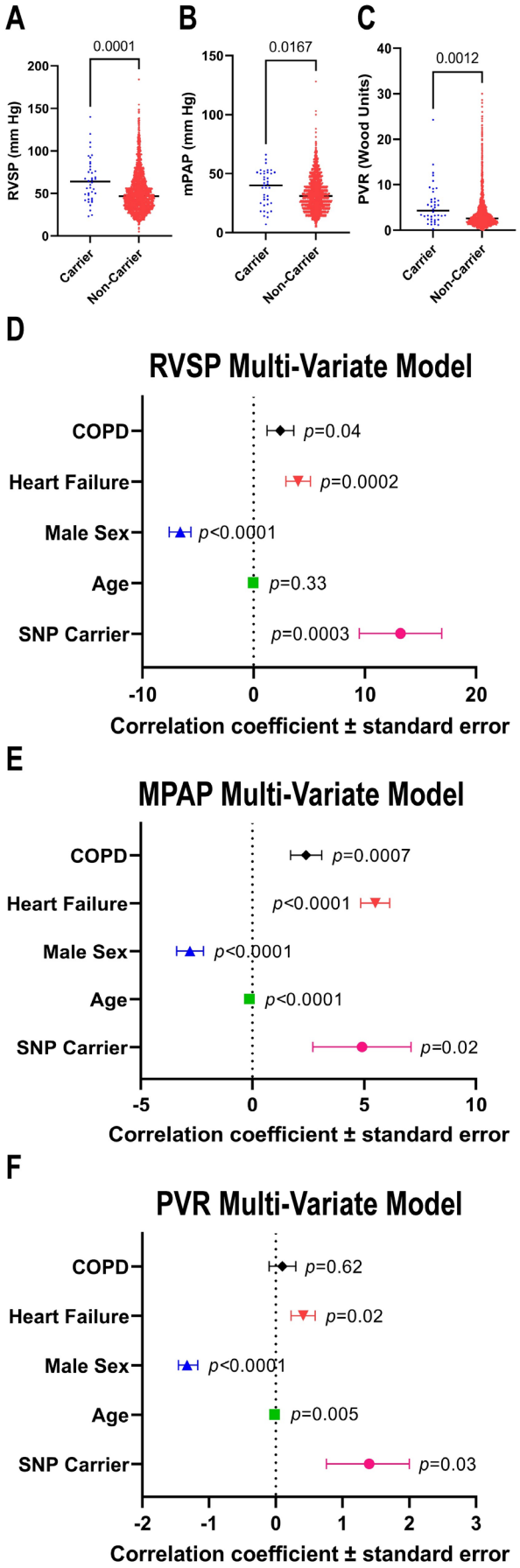
A
0.0001
RVSP (mm Hg)
200
150
100
50
0
Carrier
Non-Carrier
B
0.0167
mPAP (mm Hg)
150
100
50
0
Carrier
Non-Carrier
C
0.0012
PVR (Wood Units)
40
30
20
10
0
Carrier
Non-Carrier
D
RVSP Multi-Variate Model
COPD
p=0.04
Heart Failure
p=0.0002
Male Sex
p<0.0001
Age
p=0.33
SNP Carrier
p=0.0003
-10
0
10
20
Correlation coefficient ± standard error
E
MPAP Multi-Variate Model
COPD
p=0.0007
Heart Failure
p<0.0001
Male Sex
p<0.0001
Age
p<0.0001
SNP Carrier
p=0.02
-5
0
5
10
Correlation coefficient ± standard error
F
PVR Multi-Variate Model
COPD
p=0.62
Heart Failure
p=0.02
Male Sex
p<0.0001
Age
p=0.005
SNP Carrier
p=0.03
-2
-1
0
1
2
3
Correlation coefficient ± standard error

Figure 7: Proposed Model for the Pathogenic Role of Ferroptosis in Adverse Pulmonary Cascular Remodeling

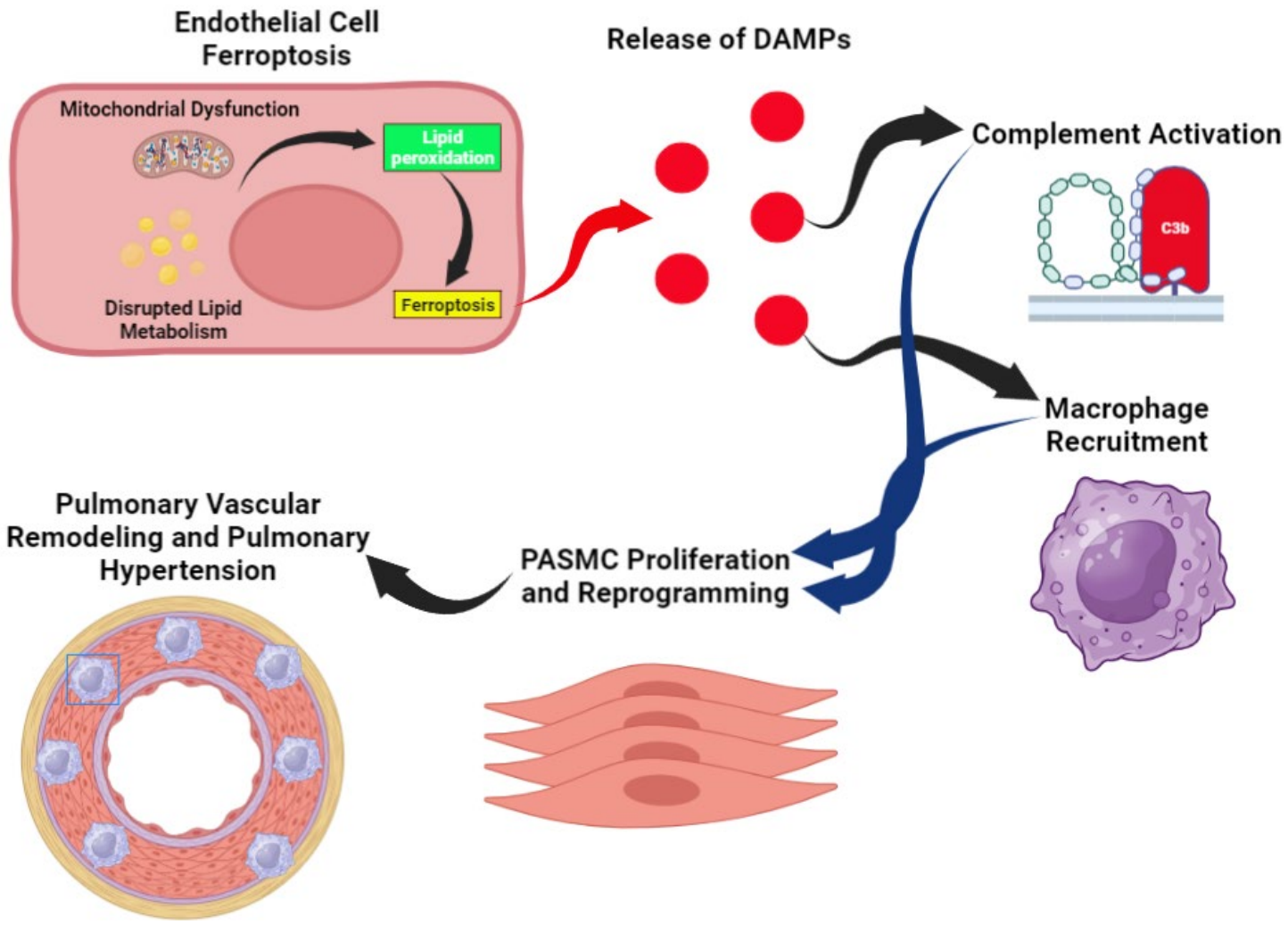

Table 1: Numerous Ferroptosis Suppressing Drugs Combat Pulmonary Hypertension in Multiple Preclinical Models

Small Molecules	Proposed Mechanisms of Ferroptosis Suppression	Animal Models With Therapeutic Effects
AICAR and metformin	AMPK Activation	Chronic hypoxia-induced pulmonary hypertension in rats, sugen-hypoxia induced pulmonary hypertension, monocrotaline rats[35]
Apocyin	Reduces reactive oxygen species required for lipid peroxidation in the NOX family of proteins	Lambs with persistent pulmonary hypertension of the newborn[36]
Deferoxamine	Iron chelation to prevent iron-dependent lipid peroxidation	Chronic hypoxia-induced pulmonary hypertension in rats[37]
MK866	Inhibits lipoxygenase-mediated lipid peroxidation	Chronic hypoxia-induced pulmonary hypertension in rats[38]
Rosiglitazone/pioglitazone	Antagonizes ACSL4-induced conversion of free fatty acids into fatty CoA esters that then become peroxidated	Monocrotaline rats, sugen-hypoxia rats, chronic hypoxia rats, $ApoE^{-/-}$ mice, transgenic TGFβ1 mice[39]
Rapamycin	mTOR Suppression	Monocrotaline-induced pulmonary hypertension in rats, chronic hypoxia-induced pulmonary hypertension in mice and rats, Sugen-hypoxia rats[40]
Vildagliptin	Blocks DPP4-mediated lipid peroxidation	Monocrotaline-induced pulmonary hypertension in rats, chronic hypoxia-induced pulmonary hypertension in rats[41]
Zileuton	Inhibits lipoxygenase-mediated lipid peroxidation	Monocrotaline pulmonary hypertension[42]

Abbreviations: AMPK: Adenosine monophosphate activate protein kinase NOX: NADPH oxidases, ACSL4: acyl-CoA synthetase long-chain family member 4, mTOR: mammalian target of rapamycin, DPP4: dipeptidyl-dippeditase-4,

References

1. Stockwell BR. Ferroptosis turns 10: Emerging mechanisms, physiological functions, and therapeutic applications. *Cell*. 2022;185:2401-2421. doi: 10.1016/j.cell.2022.06.003
2. Dixon SJ, Lemberg KM, Lamprecht MR, Skouta R, Zaitsev EM, Gleason CE, Patel DN, Bauer AJ, Cantley AM, Yang WS, et al. Ferroptosis: an iron-dependent form of nonapoptotic cell death. *Cell*. 2012;149:1060-1072. doi: 10.1016/j.cell.2012.03.042
3. Friedmann Angeli JP, Schneider M, Proneth B, Tyurina YY, Tyurin VA, Hammond VJ, Herbach N, Aichler M, Walch A, Eggenhofer E, et al. Inactivation of the ferroptosis regulator Gpx4 triggers acute renal failure in mice. *Nat Cell Biol*. 2014;16:1180-1191. doi: 10.1038/ncb3064
4. Bai T, Li M, Liu Y, Qiao Z, Wang Z. Inhibition of ferroptosis alleviates atherosclerosis through attenuating lipid peroxidation and endothelial dysfunction in mouse aortic endothelial cell. *Free Radic Biol Med*. 2020;160:92-102. doi: 10.1016/j.freeradbiomed.2020.07.026
5. Culley MK, Chan SY. Mitochondrial metabolism in pulmonary hypertension: beyond mountains there are mountains. *J Clin Invest*. 2018;128:3704-3715. doi: 10.1172/JCI120847
6. Xie SS, Deng Y, Guo SL, Li JQ, Zhou YC, Liao J, Wu DD, Lan WF. Endothelial cell ferroptosis mediates monocrotaline-induced pulmonary hypertension in rats by modulating NLRP3 inflammasome activation. *Sci Rep*. 2022;12:3056. doi: 10.1038/s41598-022-06848-7
7. Liao J, Xie SS, Deng Y, Wu DD, Meng H, Lan WF, Dai P. PRDX6-mediated pulmonary artery endothelial cell ferroptosis contributes to monocrotaline-induced pulmonary hypertension. *Microvasc Res*. 2023;146:104471. doi: 10.1016/j.mvr.2022.104471
8. Song J, Chen Y, Wang S, Dong Z, Liu X, Li X, Zhang Z, Sun L, Zhong J. Ferrostatin-1 Blunts Right Ventricular Hypertrophy and Dysfunction in Pulmonary Arterial Hypertension by Suppressing the HMOX1/GSH Signaling. *J Cardiovasc Transl Res*. 2023. doi: 10.1007/s12265-023-10423-4
9. Sun Y, Chen P, Zhai B, Zhang M, Xiang Y, Fang J, Xu S, Gao Y, Chen X, Sui X, et al. The emerging role of ferroptosis in inflammation. *Biomed Pharmacother*. 2020;127:110108. doi: 10.1016/j.biopha.2020.110108
10. Bajic G, Degn SE, Thiel S, Andersen GR. Complement activation, regulation, and molecular basis for complement-related diseases. *EMBO J*. 2015;34:2735-2757. doi: 10.15252/embj.201591881
11. Frid MG, McKeon BA, Thurman JM, Maron BA, Li M, Zhang H, Kumar S, Sullivan T, Laskowsky J, Fini MA, et al. Immunoglobulin-driven Complement Activation Regulates Proinflammatory Remodeling in Pulmonary Hypertension. *Am J Respir Crit Care Med*. 2020;201:224-239. doi: 10.1164/rccm.201903-0591OC
12. Watanabe S, Alexander M, Misharin AV, Budinger GRS. The role of macrophages in the resolution of inflammation. *J Clin Invest*. 2019;129:2619-2628. doi: 10.1172/JCI124615
13. Florentin J, Coppin E, Vasamsetti SB, Zhao J, Tai YY, Tang Y, Zhang Y, Watson A, Sembrat J, Rojas M, et al. Inflammatory Macrophage Expansion in Pulmonary Hypertension Depends upon Mobilization of Blood-Borne Monocytes. *J Immunol*. 2018;200:3612-3625. doi: 10.4049/jimmunol.1701287
14. Sutendra G, Bonnet S, Rochefort G, Haromy A, Folmes KD, Lopaschuk GD, Dyck JR, Michelakis ED. Fatty acid oxidation and malonyl-CoA decarboxylase in the vascular remodeling of pulmonary hypertension. *Sci Transl Med*. 2010;2:44ra58. doi: 10.1126/scitranslmed.3001327
15. Lee MH, Sanders L, Kumar R, Hernandez-Saavedra D, Yun X, Ford JA, Perez MJ, Mickael C, Gandjeva A, Koyanagi DE, et al. Contribution of fatty acid oxidation to the pathogenesis of pulmonary hypertension. *Am J Physiol Lung Cell Mol Physiol*. 2022;323:L355-L371. doi: 10.1152/ajplung.00039.2022
16. Sutendra G, Michelakis ED. The metabolic basis of pulmonary arterial hypertension. *Cell Metab*. 2014;19:558-573. doi: 10.1016/j.cmet.2014.01.004
17. Bertero T, Oldham WM, Cottrill KA, Pisano S, Vanderpool RR, Yu Q, Zhao J, Tai Y, Tang Y, Zhang YY, et al. Vascular stiffness mechanoactivates YAP/TAZ-dependent glutaminolysis to drive pulmonary hypertension. *J Clin Invest*. 2016;126:3313-3335. doi: 10.1172/JCI86387
18. Wertheim BM, Wang RS, Guillermier C, Hütter CV, Oldham WM, Menche J, Steinhauser ML, Maron BA. Proline and glucose metabolic reprogramming supports vascular endothelial and medial biomass in pulmonary arterial hypertension. *JCI Insight*. 2023;8. doi: 10.1172/jci.insight.163932
19. Kao CC, Wedes SH, Hsu JW, Bohren KM, Comhair SA, Jahoor F, Erzurum SC. Arginine metabolic endotypes in pulmonary arterial hypertension. *Pulm Circ*. 2015;5:124-134. doi: 10.1086/679720

20. Fang X, Wang H, Han D, Xie E, Yang X, Wei J, Gu S, Gao F, Zhu N, Yin X, et al. Ferroptosis as a target for protection against cardiomyopathy. *Proc Natl Acad Sci U S A*. 2019;116:2672-2680. doi: 10.1073/pnas.1821022116
21. Ryan JJ, Archer SL. Emerging concepts in the molecular basis of pulmonary arterial hypertension: part I: metabolic plasticity and mitochondrial dynamics in the pulmonary circulation and right ventricle in pulmonary arterial hypertension. *Circulation*. 2015;131:1691-1702. doi: 10.1161/CIRCULATIONAHA.114.006979
22. Michelakis ED, Gurtu V, Webster L, Barnes G, Watson G, Howard L, Cupitt J, Paterson I, Thompson RB, Chow K, et al. Inhibition of pyruvate dehydrogenase kinase improves pulmonary arterial hypertension in genetically susceptible patients. *Sci Transl Med*. 2017;9. doi: 10.1126/scitranslmed.aao4583
23. Huertas A, Tu L, Humbert M, Guignabert C. Chronic inflammation within the vascular wall in pulmonary arterial hypertension: more than a spectator. *Cardiovasc Res*. 2020;116:885-893. doi: 10.1093/cvr/cvz308
24. Toshner M, Church C, Harbaum L, Rhodes C, Villar Moreschi SS, Liley J, Jones R, Arora A, Batai K, Desai AA, et al. Mendelian randomisation and experimental medicine approaches to interleukin-6 as a drug target in pulmonary arterial hypertension. *Eur Respir J*. 2022;59. doi: 10.1183/13993003.02463-2020
25. Zamanian RT, Badesch D, Chung L, Domsic RT, Medsger T, Pinckney A, Keyes-Elstein L, D'Aveta C, Spychala M, White RJ, et al. Safety and Efficacy of B-Cell Depletion with Rituximab for the Treatment of Systemic Sclerosis-associated Pulmonary Arterial Hypertension: A Multicenter, Double-Blind, Randomized, Placebo-controlled Trial. *Am J Respir Crit Care Med*. 2021;204:209-221. doi: 10.1164/rccm.202009-3481OC
26. Ferrian S, Cao A, McCaffrey EF, Saito T, Greenwald NF, Nicolls MR, Bruce T, Zamanian RT, Del Rosario P, Rabinovitch M, et al. Single-Cell Imaging Maps Inflammatory Cell Subsets to Pulmonary Arterial Hypertension Vasculopathy. *Am J Respir Crit Care Med*. 2023. doi: 10.1164/rccm.202209-1761OC
27. Asosingh K, Comhair S, Mavrakis L, Xu W, Horton D, Taylor I, Tkachenko S, Hu B, Erzurum S. Single-cell transcriptomic profile of human pulmonary artery endothelial cells in health and pulmonary arterial hypertension. *Sci Rep*. 2021;11:14714. doi: 10.1038/s41598-021-94163-y
28. Xu W, Comhair SAA, Chen R, Hu B, Hou Y, Zhou Y, Mavrakis LA, Janocha AJ, Li L, Zhang D, et al. Integrative proteomics and phosphoproteomics in pulmonary arterial hypertension. *Sci Rep*. 2019;9:18623. doi: 10.1038/s41598-019-55053-6
29. Cracowski JL, Cracowski C, Bessard G, Pepin JL, Bessard J, Schwebel C, Stanke-Labesque F, Pison C. Increased lipid peroxidation in patients with pulmonary hypertension. *Am J Respir Crit Care Med*. 2001;164:1038-1042. doi: 10.1164/ajrccm.164.6.2104033
30. Schuler MH, Di Bartolomeo F, Mårtensson CU, Daum G, Becker T. Phosphatidylcholine Affects Inner Membrane Protein Translocases of Mitochondria. *J Biol Chem*. 2016;291:18718-18729. doi: 10.1074/jbc.M116.722694
31. Kagan VE, Mao G, Qu F, Angeli JP, Doll S, Croix CS, Dar HH, Liu B, Tyurin VA, Ritov VB, et al. Oxidized arachidonic and adrenic PEs navigate cells to ferroptosis. *Nat Chem Biol*. 2017;13:81-90. doi: 10.1038/nchembio.2238
32. Li J, Cao F, Yin HL, Huang ZJ, Lin ZT, Mao N, Sun B, Wang G. Ferroptosis: past, present and future. *Cell Death Dis*. 2020;11:88. doi: 10.1038/s41419-020-2298-2
33. Tamosiuniene R, Manouvakhova O, Mesange P, Saito T, Qian J, Sanyal M, Lin YC, Nguyen LP, Luria A, Tu AB, et al. Dominant Role for Regulatory T Cells in Protecting Females Against Pulmonary Hypertension. *Circ Res*. 2018;122:1689-1702. doi: 10.1161/CIRCRESAHA.117.312058
34. Perros F, Dorfmüller P, Montani D, Hammad H, Waelput W, Girerd B, Raymond N, Mercier O, Mussot S, Cohen-Kaminsky S, et al. Pulmonary lymphoid neogenesis in idiopathic pulmonary arterial hypertension. *Am J Respir Crit Care Med*. 2012;185:311-321. doi: 10.1164/rccm.201105-0927OC
35. Zhao Q, Song P, Zou MH. AMPK and Pulmonary Hypertension: Crossroads Between Vasoconstriction and Vascular Remodeling. *Front Cell Dev Biol*. 2021;9:691585. doi: 10.3389/fcell.2021.691585
36. Wedgwood S, Lakshminrusimha S, Farrow KN, Czech L, Gugino SF, Soares F, Russell JA, Steinhorn RH. Apocynin improves oxygenation and increases eNOS in persistent pulmonary hypertension of the newborn. *Am J Physiol Lung Cell Mol Physiol*. 2012;302:L616-626. doi: 10.1152/ajplung.00064.2011

37. Wong CM, Preston IR, Hill NS, Suzuki YJ. Iron chelation inhibits the development of pulmonary vascular remodeling. *Free Radic Biol Med*. 2012;53:1738-1747. doi: 10.1016/j.freeradbiomed.2012.08.576
38. Voelkel NF, Tuder RM, Wade K, Höper M, Lepley RA, Goulet JL, Koller BH, Fitzpatrick F. Inhibition of 5-lipoxygenase-activating protein (FLAP) reduces pulmonary vascular reactivity and pulmonary hypertension in hypoxic rats. *J Clin Invest*. 1996;97:2491-2498. doi: 10.1172/JCI118696
39. Hansmann G, Calvier L, Risbano MG, Chan SY. Activation of the Metabolic Master Regulator PPARγ: A Potential PIOneering Therapy for Pulmonary Arterial Hypertension. *Am J Respir Cell Mol Biol*. 2020;62:143-156. doi: 10.1165/rcmb.2019-0226PS
40. Babicheva A, Makino A, Yuan JX. mTOR Signaling in Pulmonary Vascular Disease: Pathogenic Role and Therapeutic Target. *Int J Mol Sci*. 2021;22. doi: 10.3390/ijms22042144
41. Xu J, Wang J, He M, Han H, Xie W, Wang H, Kong H. Dipeptidyl peptidase IV (DPP-4) inhibition alleviates pulmonary arterial remodeling in experimental pulmonary hypertension. *Lab Invest*. 2018;98:1333-1346. doi: 10.1038/s41374-018-0080-1
42. Jones JE, Walker JL, Song Y, Weiss N, Cardoso WV, Tuder RM, Loscalzo J, Zhang YY. Effect of 5-lipoxygenase on the development of pulmonary hypertension in rats. *Am J Physiol Heart Circ Physiol*. 2004;286:H1775-1784. doi: 10.1152/ajpheart.00281.2003